ISSN 0018-151X, High Temperature, 2021, Vol. 59, No. 1, pp. 90–98. © Pleiades Publishing, Ltd., 2021.
Russian Text © The Author(s), 2021, published in Teplofizika Vysokikh Temperatur, 2021, Vol. 59, No. 1, pp. 100–108.

HEAT AND MASS TRANSFER AND PHYSICAL GASDYNAMICS

Numerical Study of the Influence of Spherically Blunted Cone Oscillations during a Supersonic Air Flow around on the Characteristics of Conjugate Heat and Mass Transfer

K. N. Efimov[a], V. A. Ovchinnikov[a], and A. S. Yakimov[a, *]

[a] *National Research Tomsk State University, Tomsk, 634050 Russia*

**e-mail: yakimovas@mail.ru*

Received November 6, 2019; revised May 15, 2020; accepted October 14, 2020

Abstract—This work examines the action of the fluctuations of a body in a supersonic air flow on coupled heat and mass transfer in a heat-protection material in the presence of injected thermochemical destruction products and heat and mass transfer between the body and the incoming flow. The results of a numerical study of a spatial supersonic flow around a spherically blunted cone oscillating in the pitch plane are presented. The influence of the oscillations of a body with angular velocity of 0–100 deg/s on the surface temperature and heat transfer characteristics is considered.

DOI: 10.1134/S0018151X20060073

INTRODUCTION

Flying vehicles undergo a strong thermal action that alters their shape and aerodynamic characteristics during motion at hypersonic velocities in dense layers of the Earth's atmosphere. The presence of fluctuating motions change the flow conditions and thermal state of the body as compared to their absence. The influence of variable angles of attack on aerodynamic characteristics of axisymmetric bodies exposed to the air flow was studied earlier (e.g., in [1, 2]). In connection with this, it is interesting to analyze the influence of such oscillatory motions on the thermal state of the body when it interacts with high-enthalpy flows. During the flow around a body with a constant angle of attack [3, 4], the difference between heat fluxes on the leeward and windward sides can be very considerable, which leads to nonuniform heating. To reduce this effect, supersonic flying vehicles can be put into rotational and oscillatory motion. The interrelated character of thermal and aerodynamic processes makes it necessary in the mathematical simulation to solve the problem in conjugate formulation [5]. The influence of body rotation around an axis on conjugate heat and mass transfer characteristics at supersonic flow around the body was studied in [6–8].

In this work, the gas flow is described by boundary layer equations with allowance for the laminar and turbulent flow regimes. A system of conservation equations for a porous medium is written to describe the thermal state of the body. Different destructive processes on the conical part of the body surface in a flow and the filtration of the cooling gas in pores on the spherical bluntness are taken into account. The problem is solved in the conjugate formulation [5, 9] because this makes it possible to significantly increase the accuracy of the determination of the aerodynamic and thermal characteristics as compared with separate estimations of the aerodynamics, thermochemical destruction, and parameters of the body motion.

FORMULATION OF THE PROBLEM

The relaxation times in the gaseous and condensed phases were estimated in [5, 9]. Based on these estimations, the characteristics of conjugate heat and mass transfer are found from the solution of quasi-stationary equations of the spatial boundary layer at different flow regimes. The thermal state of the porous shell is determined from the solution of the nonstationary equation of energy conservation for a porous spherical bluntness and quasi-stationary equation for the filtration rate of the cooling gas in pores within the framework of the single-temperature model.

For the model of chemical-equilibrium air according to the passivity hypothesis and the Lewis numbers being unity for all components, the system of equations of the spatial boundary layer in the natural coordinate system associated with the outer surface of the shell exposed to a flow has the form [3, 8] (Fig. 1)

$$\frac{\partial}{\partial s}(\rho u r_w) + \frac{\partial}{\partial n}(\rho v r_w) + \frac{\partial}{\partial \eta}(\rho w) = 0, \tag{1}$$

$$\rho\left(u\frac{\partial u}{\partial s} + v\frac{\partial u}{\partial n} + \frac{w}{r_w}\frac{\partial u}{\partial \eta} - \frac{w^2}{r_w}\frac{\partial r_w}{\partial s}\right) = -\frac{\partial P_e}{\partial s} + \frac{\partial}{\partial n}\left(\mu_\Sigma \frac{\partial u}{\partial n}\right), \tag{2}$$

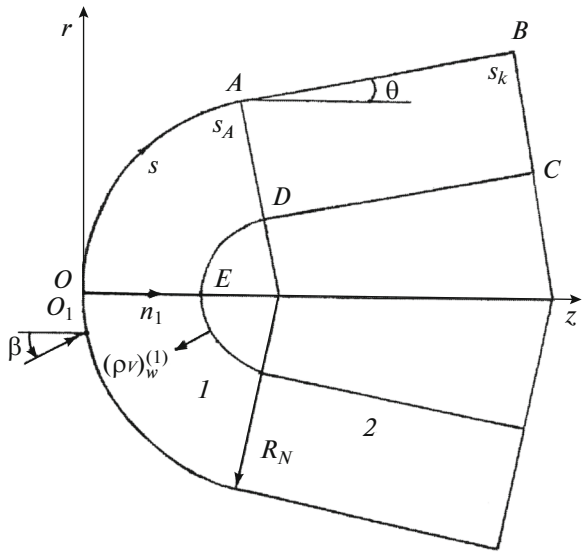

Fig. 1. Scheme of the flow around the body: (*1*) porous spherical bluntness and (*2*) conical part of the body (carbon composite or graphite).

$$\rho\left(u\frac{\partial w}{\partial s}+v\frac{\partial w}{\partial n}+\frac{w}{r_w}\frac{\partial w}{\partial \eta}+\frac{uw}{r_w}\frac{\partial r_w}{\partial s}\right) = -\frac{1}{r_w}\frac{\partial P_e}{\partial \eta}+\frac{\partial}{\partial n}\left(\mu_\Sigma\frac{\partial w}{\partial n}\right), \tag{3}$$

$$\rho\left(u\frac{\partial H}{\partial s}+v\frac{\partial H}{\partial n}+\frac{w}{r_w}\frac{\partial H}{\partial \eta}\right) = \frac{\partial}{\partial n}\left\{\frac{\mu_\Sigma}{\mathrm{Pr}_\Sigma}\left[\frac{\partial H}{\partial n}+(\mathrm{Pr}_\Sigma-1)\frac{\partial}{\partial n}\left(\frac{u^2+w^2}{2}\right)\right]\right\}, \tag{4}$$

$$P=\rho h(\gamma_{\mathrm{ef}}-1)/\gamma_{\mathrm{ef}},\quad P=P_e(s,\eta),\qquad H=h+\left(u^2+w^2\right)/2, \tag{5}$$

$$\mu_z=\mu+\Gamma\mu_T,\quad \mathrm{Pr}_\Sigma=\frac{(\mu+\Gamma\mu_T)\,\mathrm{Pr}\,\mathrm{Pr}_T}{\mu\,\mathrm{Pr}_T+\Gamma\,\mu_T\,\mathrm{Pr}}.$$

For the porous spherical shell ($0 < s < s_A$) and one-dimensional process of injected gas filtration in the direction of the normal to the surface in the considered coordinate system associated with the axis of symmetry of the body, we have [9, 10] at $0 \le \eta < 2\pi$

$$\frac{\partial(\rho_2\varphi v r_1 H_1)}{\partial n_1}=0, \tag{6}$$

$$(\rho c_p)_1(1-\varphi)\frac{\partial T_1}{\partial t}=\frac{1}{r_1H_1}\left\{\frac{\partial}{\partial n_1}\left[r_1H_1\lambda_1(1-\varphi)\frac{\partial T_1}{\partial n_1}\right]+\frac{\partial}{\partial s}\left[\frac{r_1\lambda_1}{H_1}(1-\varphi)\frac{\partial T_1}{\partial s}\right]+\frac{\partial}{\partial \eta}\left[\frac{H_1\lambda_1}{r_1}(1-\varphi)\frac{\partial T_1}{\partial \eta}\right]\right\} + c_{p2}\,(\rho v)_w^{(1)}\frac{r_{1w}}{r_1H_1}\frac{\partial T_1}{\partial n_1}, \tag{7}$$

$$A\mu v+B\rho_2\varphi v|v|=-\frac{\partial P}{\partial n_1}, \tag{8}$$

$$P=\frac{\rho_2RT_1}{M},\quad H_1=\frac{R_N-n_1}{R_N},\quad \bar{s}=\frac{s}{R_N},\qquad r_1=(R_N-n_1)\sin(\bar{s}),\quad \mu\sim\sqrt{T_1},\quad \lambda_1\sim\sqrt{T_1},\qquad \varphi=\mathrm{const}. \tag{9}$$

For the conical part of the body ($s_A < s < s_k$), the equations of energy and mass conservation in the moving coordinate system are written according to the mathematical models presented in [6, 10] at $0 \le \eta < 2\pi$:

$$\rho_c c_p\left(\frac{\partial T}{\partial t}-\psi\frac{\partial T}{\partial n_1}\right)+c_{p2}G\frac{\partial T}{\partial n_1}=\frac{\partial}{\partial n_1}\left(\lambda\frac{\partial T}{\partial n_1}\right)+\frac{\partial}{\partial s}\left(\lambda\frac{\partial T}{\partial s}\right)+\frac{1}{r_2^2}\frac{\partial}{\partial \eta}\left(\lambda\frac{\partial T}{\partial \eta}\right)-Q_c\frac{d\rho_c}{dt}, \tag{10}$$

$$\frac{d\rho_c}{dt}=\left(\frac{\partial\rho_c}{\partial t}-\psi\frac{\partial\rho_c}{\partial n_1}\right)=\begin{cases}-k_c\rho_{c0}\left(\dfrac{\rho_c-\rho_{c*}}{\rho_{c0}}\right)\exp\left(-\dfrac{E_c}{RT}\right), & \rho_c>\rho_{c*},\\ 0, & \rho_c\le\rho_{c*},\end{cases} \tag{11}$$

$$G=\int_0^{l_1}\frac{d\rho_c}{dt}dn_1,\quad r_2=(R_N-n_1)\cos\theta+(s-s_A)\sin\theta,$$

$$l=L-x(t),\quad x(t)=\int_0^t\psi d\tau,\quad (\rho v)_{1w}=G_w,$$

$$(\rho v)_w^{(2)}=(\rho v)_{1w}+(\rho v)_{2w}+(\rho v)_{3w},\qquad \psi=\sum_{i=2}^{3}\frac{(\rho v)_{iw}}{\rho_{cw}}. \tag{12}$$

In contrast to [6–8], periodic oscillations of the angle of attack in the pitch plane are considered in this paper. This motion is described by the expression

$$\beta(t)=\begin{cases}\beta_m-|\omega_f t-\beta_m|-(i-1)B_f,\\ (i-1)B_f\le t<B_f\,i/2,\\ |\omega_f t-3\beta_m|-\beta_m-B_f\,i/2,\\ B_f\,i/2\le t<B_f i.\end{cases} \tag{13}$$

In formula (13), t is the duration of the process, $i = 1, 2\ldots$, $B_f = 4\beta_m/\omega_f$ is the fluctuation period, ω_f is the angular velocity of the angle of attack β, and β_m is the maximum angle of attack.

The following assumptions are introduced: (i) the characteristic linear velocity of body oscillation is much less than the velocity of the incoming flow $\Omega_f = \omega_f R_N/V_\infty \ll 1$; (ii) the characteristic time of the oscillatory process is much greater than the relaxation time of the gaseous phase ($t_\omega \gg t_a$, $t_\omega = 4\beta_m/\omega_f$, $t_a =$

R_N/V_∞). This allows one to use boundary layer equations in the quasi-stationary form.

The initial conditions are

$$T_1|_{t=0} = T|_{t=0} = T_0, \quad \rho_c|_{t=0} = \rho_{c0}. \tag{14}$$

The boundary conditions in the gaseous phase are written as follows: at the outer boundary of the boundary layer at $n \to \infty$,

$$u \to u_e(s,\eta), \quad w \to w_e(s,\eta), \quad h \to h_e(s,\eta), \tag{15}$$

where u_e, w_e, h_e, and P_e in (5) are determined from the solution of the system of Euler equations [11];

on the surface of the body exposed to the flow at $n = 0$,

$$u(s,\eta) = 0, \quad w = 0, \quad v = v_w, \quad (0 < s < s_A). \tag{16}$$

On the outer surface of the shell in the flow ($n = n_1 = 0$), the following conditions take place [6, 9] at $0 \le \eta < 2\pi$:

$$\frac{\mu}{\mathrm{Pr}}\left(\frac{\partial h}{\partial n}\right)\Big|_w - (1-\varphi)\varepsilon_1\sigma T_{1w}^4 = -\lambda_1(1-\varphi)\left(\frac{\partial T_1}{\partial n_1}\right)\Big|_w, \quad 0 < s < s_A, \tag{17}$$

$$-\lambda\frac{\partial T}{\partial n_1}\Big|_{n_1=0-x(t)} = \frac{\mu}{\mathrm{Pr}}\left(\frac{\partial h}{\partial n}\right)\Big|_w - (h_w - h_c)\sum_{i=2}^{3}(\rho v)_{iw} - (\rho v)_{1w}(h_w - h_g) - \varepsilon\sigma T_w^4, \quad s_A \le s \le s_k. \tag{18}$$

On the inner surface of the hemisphere and conical part, the following relationships are written [9]:

$$-\lambda_1(1-\varphi)\frac{\partial T_1}{\partial n_1}\Big|_{n_1=L} = \delta(T_{1,L} - T_0), \quad 0 < s < s_A, \tag{19}$$

$$\rho_c|_{n_1=l} = \rho_{c0}, \quad \lambda\frac{\partial T}{\partial n_1}\Big|_{n_1=\ell} = 0, \quad s_A \le s \le s_k. \tag{20}$$

On the sphere–cone transition ring $s = s_A$, conditions of perfect contact are used, at $s = s_k$, the adiabatic condition

$$\frac{\lambda_1(1-\varphi)}{H_1}\frac{\partial T_1}{\partial s}\Big|_{s=s_A-0} = \lambda\frac{\partial T}{\partial s}\Big|_{s=s_A+0}, \quad T_1|_{s=s_A-0} = T|_{s=s_A+0}, \quad \frac{\partial T}{\partial s}\Big|_{s=s_k} = 0. \tag{21}$$

On the outer and inner surfaces of the spherical bluntness region, equality of pressures in pores and in the external environment takes place:

$$P_w|_{n_1=0} = P_e(s,\eta), \quad P|_{n_1=L} = P_L. \tag{22}$$

In the absence of the flow symmetry plane, the following periodicity conditions take place:

$$T_1(t,n_1,s,\eta) = T_1(t,n_1,s,\eta+2\pi), \quad T(t,n_1,s,\eta) = T(t,n_1,s,\eta+2\pi). \tag{23}$$

At the interface at $s \ge s_A$, the following kinetic scheme of nonequilibrium chemical reactions was considered ($T_w \le 4000$ K) [9, 10, 12]:

$$\mathrm{C} + \mathrm{O}_2 \to \mathrm{CO}_2, \quad 2\mathrm{C} + \mathrm{O}_2 \to 2\mathrm{CO}, \quad \mathrm{C} + \mathrm{O} \to \mathrm{CO}, \quad \mathrm{C} + \mathrm{CO}_2 \to 2\mathrm{CO}, \quad 2\mathrm{O} + \mathrm{C} \to \mathrm{O}_2 + \mathrm{C}, \quad 2\mathrm{N} + \mathrm{C} \to \mathrm{N}_2 + \mathrm{C}, \quad \mathrm{C} \leftrightarrow \mathrm{C}_1, \quad \mathrm{C} \leftrightarrow \mathrm{C}_3. \tag{24}$$

The molar and mass rates of development of these chemical reactions (24) and the expression for the ablation rate were described in detail in [5, 9]; the formulas for $(\rho v)_{2w}$ and $(\rho v)_{3w}$ from (12) have the form

$$(\rho v)_{2w} = \rho_w\left[\left(\frac{m_6}{m_2} - 1\right)c_{2w}B_1 + \left(2\frac{m_5}{m_2} - 1\right)c_{2w}B_2 + \left(\frac{m_5}{m_1} - 1\right)c_{1w}B_3 + \left(2\frac{m_5}{m_6} - 1\right)c_{6w}B_4\right];$$

$$(\rho v)_{3w} = \sum_{i=7}^{8}\frac{m_i A_{ci}(P_{ci}^* - P_{ci})}{(2\pi R T_w m_i)^{0.5}}, \quad i = 7,8;$$

$$P_{ci}^* = 10^5\exp(D_i - E_i/T_w); \quad B_i = k_{iw}\exp(-E_{iw}/RT_w), \quad i = \overline{1,4}; \quad P_{ci} = P_e c_{iw}\, m_w/m_i, \quad i = 7,8; \tag{25}$$

$$\rho_w = P_e m_w/(RT_w), \quad h_w = \sum_{i=1}^{8} h_i c_{iw}, \quad m_w^{-1} = \sum_{i=1}^{8} c_{iw}/m_i;$$

$$c_{p2} = b_1 + b_2 T, \quad h_g = \int_0^T c_{p2}\,dT.$$

In Eqs. (24) and (25), the order number of the components corresponds to the following order of their enumeration: O, O_2, N, N_2, CO, CO_2, C_1, and C_3. C designates solid-phase carbon belonging to the thermal protection coating material. In the boundary layer, there are four components: O, O_2, N, and N_2, which participate in two equilibrium chemical reactions: $O_2 \leftrightarrow 2O$ and $N_2 \leftrightarrow 2N$. At the interface of the condensed and gaseous phases, four components are present: CO, CO_2, C_1, and C_3. They appear in six heterogeneous combustion and sublimation reactions from (24). Two reactions of catalytic recombination of O_2 and N_2 components are also taken into account.

The balance relations for mass concentrations of components (c_{iw}) are written with Fick's law for diffusion flows and the analogy between heat and mass transfer processes [10]:

$$J_{iw} + (\rho v)_w^{(2)} c_{iw} = R_{iw}, \quad i = \overline{1,8}, \quad J_{iw} = \gamma_i(c_{iw} - c_{ie}), \quad \gamma_i = \alpha/c_p,$$

where α/c_p and γ_i are the heat transfer and mass transfer coefficients, respectively. It is assumed that products of destruction poorly dilute the air mixture in the boundary layer. This allows one to use the aforementioned formulation for the equations in the boundary layer.

Hereinafter, u, v, and w are components of the mass-average velocity vector in the natural coordinate system (s, n, η); Γ is the intermittency factor; H and m are the total enthalpy and molecular mass; R_N is the spherical bluntness radius; r_w, r_i ($i = 1, 2$) and H_1 are the Lamé coefficients; h and $(\rho v)_w^{(1)}$ are the enthalpy and rate of the coolant gas outflow from the spherical bluntness surface; ρ is the density; μ is the dynamic viscosity; P is pressure; T is temperature; $(\rho v)_w^{(2)}$ is the total mass ablation from the carbon surface of the conical part of the body; A and B are the viscous and inertial coefficients in the nonlinear Darcy law (8); v is the filtration rate; φ is the porosity of the spherical bluntness; c_p is the coefficient of heat capacity at constant pressure; λ is the heat conduction coefficient; R is the universal gas constant; M is the molecular mass of gas in a porous shell; L is the shell thickness; θ is the cone angle; β is the angle of attack; n_1 is the normal to the surface directed inside the shell; ψ is the is the linear velocity of displacement of the destruction surface; $x(t)$ is the interface between the gaseous and condensed phases; (the burnout depth); E_{iw}, k_{iw} ($i = 1,\ldots,4$) are the activation energy and preexponent of the ith heterogeneous reaction of the shell of the conical part of the body; k_c, E_c, and Q_c are the preexponent, activation energy, and heat effect of a pyrolytic reaction; H_∞ and V_∞ are the height and velocity of the incoming flow at infinity; σ is the Stefan–Boltzmann constant; ε is the surface emissivity; G is the mass ablation of carbon composite pyrolysis products; δ is the heat transfer coefficient on the inner cold surface of the spherical shell; and Pr is the Prandtl number.

The subscripts e, $e0$, and w correspond to values at the outer boundary of the boundary layer, at the outer boundary at the deceleration point, and on the surface of the body exposed to the flow; the subscripts (1) and (2) are for the characteristics of the frame and gas on the sphere; g is for the gaseous phase on the conical part of the surface; ∞ is for the magnitude of the incoming gas flow at infinity; T and 0 are for the characteristic of the turbulent transport and initial conditions; L is for the inner shell of the spherical part of the body; k is for the peripheral section of the shell; the superscripts (1) and (2) denote characteristics related to the coolant flow rate on the porous hemisphere and surface chemical reactions on the conical part of the body; the overbar means a dimensionless parameter; z denote the time of termination of the thermal action; ef denotes the effective value; m is for the maximum value; and c refers to the carbon composite.

CALCULATION METHOD AND INITIAL DATA

The system of equations (1)–(4), (6)–(8), (10), and (11) with the initial and boundary conditions (14)–(23) is solved numerically. The system of equations for the spatial boundary layer was solved in Dorodnitsyn type variables with allowance for the laminar, transitional, and turbulent flow regions. The turbulent flow was described with the two-layer model of the turbulent boundary layer [13, 14]. The considered three-layer algebraic turbulence model takes into account the laminar viscous sublayer, the turbulent internal core described by the van Driest–Cebeci formula [14], and the outer region, in which the Spalding formula [13] is used. The intermittency factor and transition from the laminar to turbulent flow regime was described with the Dhawan–Narasimha formula [15]. In the numerical integration, Pr = 0.72 and $\mathrm{Pr}_T = 1$. For the boundary layer equations, combined difference schemes were obtained with the iterated-interpolation method [16]; they provide the fitting of the sought characteristics at the boundary of the laminar sublayer and turbulent core and take into account the behavior of μ_T transverse to the boundary layer. The parameters of the technique [15], in particular, the position of points of the loss in stability of the laminar flow and transition to the turbulent flow, were chosen proceeding from experimental data [17, 18], which were also used to test the described boundary layer model and to demonstrate its good applicability.

The numerical solution of the three-dimensional equations (7) and (10) was performed via splitting [19] with the use of an implicit, absolutely stable, monotonous difference scheme with a total approximation error $O(\tau + H_{n_1}^2 + H_s^2 + H_\eta^2)$, where H_{n_1}, H_s, and H_η are the space steps along the n_1, s, and η coordinates, respectively, and τ is the time step. The program of numerical calculations in the porous body was verified with a sequence of bunching spatial meshes with spatial steps $h_1 = h_{n_1} = 10^{-3}$ m, $h_2 = h_{s1} = 0.925 \times 10^{-2}$ (on the sphere), $h_3 = h_{s2} = 10^{-2}$ (on the cone), $h_4 = h_\eta = 0.087$, as well as the quantities $H_{1,i} = 2 \times h_i$, $H_{2,i} = h_i$, $H_{3,i} = h_i/2$, and $H_{4,i} = h_i/4$, $i = 1$–4. The frame temperature was measured along the depth of the body at different instants of time. The problem in all versions was solved with a variable time step chosen to provide the required accuracy, which was equal for all space steps. The difference between the relative errors in temperature decreased to the instant of time $t = t_z$ and was equal to $\Delta_1 = 10.3\%$, $\Delta_2 = 6.5\%$, and $\Delta_3 = 3.4\%$. The calculation results presented below were obtained for space steps $H_{3,i} = h_i/2$, $i = 1$–4.

The processes of the interaction of high-enthalpy air flows with graphite surfaces were tested based on

the results of theoretical [20] and generalized experimental studies [21].

The quasi-stationary continuity equation (6) $(\rho v)_w r_{1w}/(H_1 r_1) = -\rho_2 \varphi v$ (the minus sign is due to the fact that the normal coordinate n_1 is directed inward the body (see Fig. 1) and the coolant flows in the opposite direction), jointly with the first expression of (9), the nonlinear Darcy law (8), and the boundary conditions (22), can be integrated and the gas flow rate and the pressure in region *1* can be found [9]:

$$(\rho v)_w(s,\eta) = \frac{\left[2B(P_L^2 - P_w^2)\varphi MD_L/R + E_L^2\right]^{0.5} - E_L}{2BD_L},$$

$$P(n_1,s,\eta) = \{P_w^2 + 2R(\rho v)_w[B(\rho v)_w D + E]/M\varphi\}^{0.5},$$

$$D(n_1,s,\eta) = \int_0^{n_1} T_1\left(\frac{r_{1w}}{r_1 H_1}\right)^2 dy,$$

$$E(n_1,s,\eta) = A\int_0^{n_1} \mu T_1 \frac{r_{1w}}{r_1 H_1} dy.$$

The pressure on the inner "cold" surface of the plate L is specified in the form

$$P_L = kP_{e0},$$

where k is a constant. This ensured the necessary flow rate of the coolant (in particular, the melting point of a frame made of a porous metal was not reached [10, 22]) within the section of thermal action from $t = 0$ to $t = t_z$.

The chemically balanced airflow around a spherically blunted cone with a semiapex angle of $\theta = 15°$ with a variable angle of attack $\beta_m \le \beta \le \beta_m$, $\beta_m = 10°$ was calculated for the following conditions [11], which correspond to parameters $H_\infty = 2.3 \times 10^4$ m, $V_\infty =$ 3000 and 5000 m/s, $R_N = 0.1$ m, $L_0 = 0.02$ m, and $k = 2$. The characteristic values at the given parameters of the problem are the oscillatory process time $t_\omega =$ 0.4 s, the relaxation time for the gaseous phase $t_a = 3.3 \times 10^{-5}$ s, and the Strouhal number $\mathrm{St} = t_a/t_\omega = 8.25 \times 10^{-5}$. The kinetic constants (25) of heterogeneous reactions (24) were taken from [9], and the graphite enthalpy h_c was calculated with formula [23]. The effective adiabatic exponent γ_{ef} in the first formula of (5) was determined according to [11]. The thermophysical coefficients for the carbon material of the conical shell are known from [9]; those for porous steel are known from [24]. For graphite of the conical part of the body, Eq. (10) is solved at $Q_c = 0$ and $G = 0$.

The results presented below were obtained at $h_{e0} = 4.7197 \times 10^6$ and 1.272×10^7 J/kg, $\varphi = 0.34$, $T_0 =$ 300 K, $b_1 = 965.5$, $b_2 = 0.147$, $M = 29$ kg/kmol, $\sigma = 5.67 \times 10^{-8}$ W/(m^2 K^4), $\varepsilon = 0.9$, $\rho_{c0} = 1400$ kg/m^3, $\rho_{c*} = 1300$ kg/m^3, $k_c = 3.15 \times 10^6$ s^{-1}, $E_c = 8.38 \times 10^4$ J/mol, $Q_c = 1.26 \times 10^6$ J/kg, and $t_z = 40$ s. The thermophysical characteristics of the porous bluntness corresponded to porous steel: $\varepsilon_1 = 0.8$, $\lambda_1 = 2.92 + 4.5 \times 10^{-3} T_1$ W/(m K), $\rho_1 c_{p1} = (1252 + 0.544T_1) \times 10^3$ J/(K m^3) [24], $A = 2.3 \times 10^{11}$ 1/ m^2, and $B = 5.7 \times 10^5$ 1/m. The thermophysical characteristics of the conical part of the body correspond to carbon composite [4, 9] or VPP solid graphite [25].

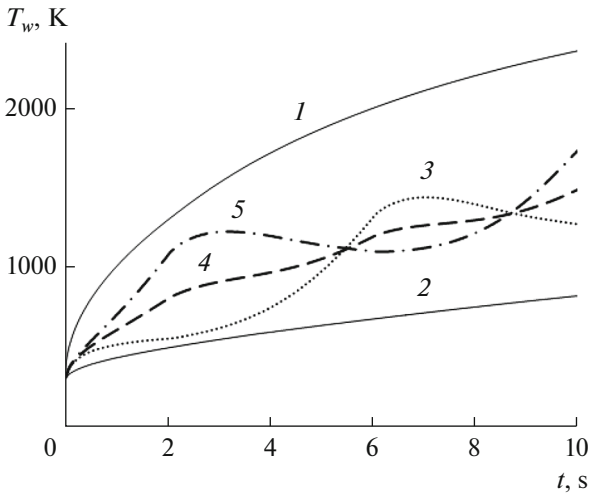

Fig. 2. Dependence of the graphite surface temperature in the cross section $s/R_N = 5.0$ at $V_\infty = 5000$ m/s: $\omega_f =$ 0 (*1*, *2*) and (*3*–*5*) 5 deg/s.

RESULTS OF NUMERICAL SOLUTION AND ANALYSIS

In what follows, the results refer to the cross section $s/R_N = 5.0$, which is on the conical part of the body. If the cross-section coordinate is chosen in this way, predetached states are not observed on the leeward part of the body at any time of the process. Due to the short thermal relaxation times of carbon composites [7], graphite is more convenient for the illustration of nonstationary thermal processes (Figs. 2–7) that appear due to the oscillatory motion and strong aerodynamic heating. Nevertheless, the results in Figs. 2–7 qualitatively reflect the influence of oscillations on the carbon composite. Figure 8 presents integrated quantitative comparisons of graphite and carbon composite.

Figure 2 shows the time dependence of the surface temperature for the body of graphite at an incoming flow velocity of $V_\infty = 5000$ m/s and a fixed angle of attack $\beta = \beta_m = 10°$ ($\omega_f = 0$): curves *1*–*2* and $\omega_f =$ 5 deg/s (curves *3*–*5*). In the absence of the oscillatory process, a monotonic growth of temperature is observed at points $\eta = 180°$ (curve *1*) and 0° (curve *2*).

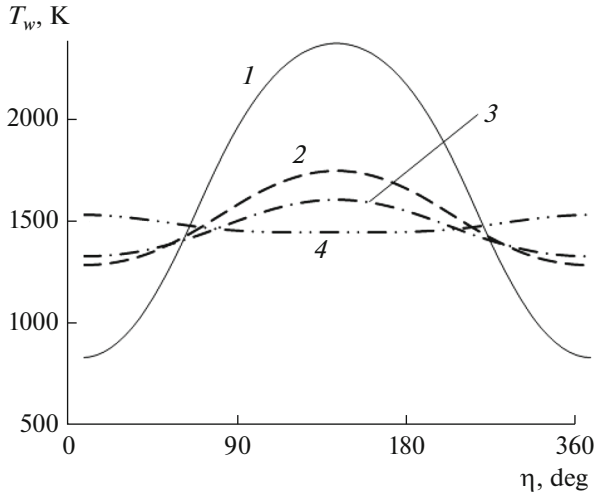

Fig. 3. Distribution of the graphite surface temperature over the circumferential coordinate at V_∞ = 5000 m/s: ω_f = 0 (*1*), (*2*) 5, (*3*) 10, and (*4*) 100 deg/s.

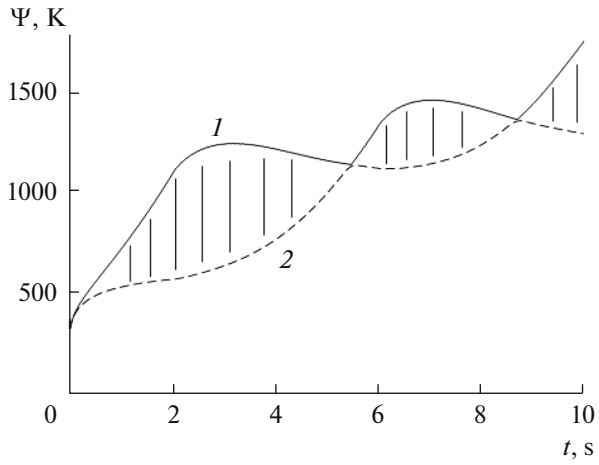

Fig. 4. Generators of the family of curves $T_{w\eta}(t)$ at V_∞ = 5000 m/s and ω_f = 5 deg/s for the graphite material on the conical part of the shell.

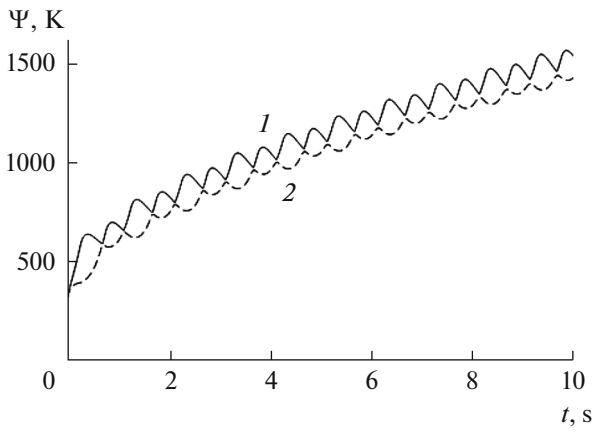

Fig. 5. Generators of the family of $T_{w\eta}(t)$ curves at V_∞ = 5000 m/s and ω_f = 40 deg/s for graphite.

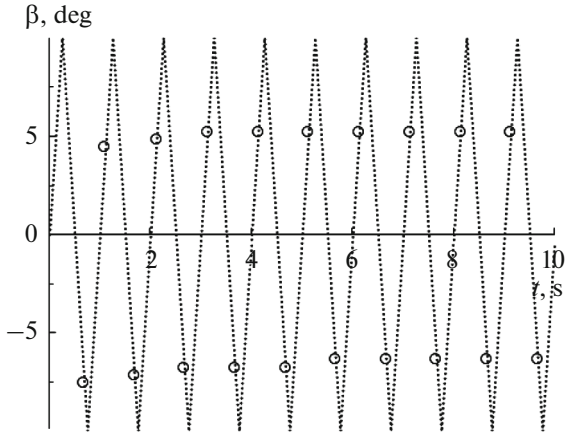

Fig. 6. Time dependence of the angle of attack: the dots are time instants of the transition to the isothermal regime at V_∞ = 5000 m/s and ω_f = 40 deg/s for graphite.

In the presence of the oscillatory motion (curves *3–5*), the surface temperature nonmonotonically varies at points with coordinates η = 0, 90, and 180° which are in correspondence with curves *3–5*. At the same time, curves *3–5* periodically intersect at certain time instants. As seen from Fig. 2, the oscillatory motion leads to a decrease in the temperature difference from 1563 to 463 K at t = 10 s.

This can be also demonstrated by distributions of the graphite surface temperature along the circumferential coordinate; they are shown in Fig. 3 for the time instant t = 10 s. Here, curves *1–4* are in correspondence with ω_f = 0, 5, 10, and 100 deg/s. It is seen from Fig. 3 that η = 180° at this instant corresponds to the windward side for curves *1–3* and to the leeward side for curve *4*. The maximum temperature difference of 1538 K on the surface over the circumferential coordinate is reached in the absence of body oscillations ω_f = 0 deg/s (Fig. 3, curve *1*). With an increase in the angular velocity of oscillations ω_f to 100 deg/s, the difference of temperatures decreases to 83 K.

Let us consider 37 time curves of $T_{w\eta}(t)$ describing the variation in surface temperatures of the conical part of graphite at points η = 0, 5, ..., 175, and 180° of the studied cross section *s*. Let us introduce functions $\Psi_{\min}(t)$ and $\Psi_{\max}(t)$, which are the envelopes of the family of 37 $T_{w\eta}(t)$ curves obtained from the solution of

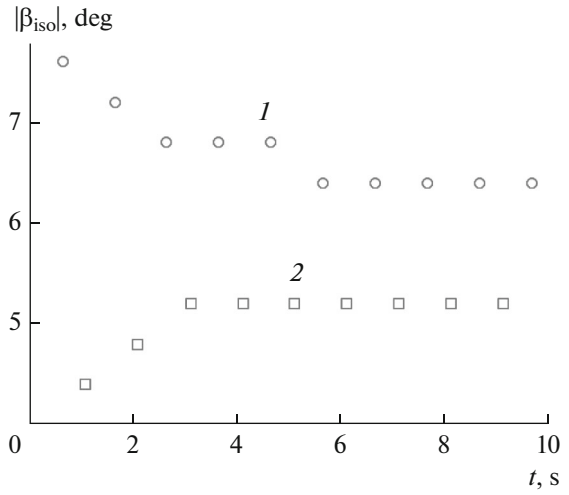

Fig. 7. Modulus of the angle of attack at time instants of the transition to the isothermal regime at $\omega_f = 40$ deg/s and $V_\infty = 5000$ m/s for graphite: (*1*) $\beta > 0$ and (*2*) $\beta < 0$.

the conjugate problem at fixed ω_f and s/R_N. Figures 4 and 5 show the dependences $\Psi_{max}(t)$ (curve *1*) and $\Psi_{min}(t)$ (curve *2*) for the angular velocities of body oscillations $\omega_f = 5$ and 40 deg/s, respectively. It is seen from Figs. 4 and 5 that, at certain time instants, the solid and dashed curves have common points. This means that the surface in the cross section s/R_N at these time instants becomes close to isothermal.

It is known that the surface temperature at $\omega_f = 0$ is constant along the circumferential coordinate η at zero angle of attack [3]. In the case of the oscillatory motion, the temperature approaches a constant value in a period of time, after the angle of attack β passes the zero value (Fig. 6). As seen from Figs. 4–6, the transition to the local isothermal regime is of a cyclic character and depends on the angular velocity of oscillations ω_f. It follows from results of calculations at $\omega_f = 40$ deg/s that the surface becomes close to isothermal with irregular cyclicity at different angles of attack β_{iso} presented in Fig. 7. As seen from this figure, the value of $|\beta_{iso}|$ decreases with time and is influenced by the sign of the angle of attack. At $\beta < 0$, the value of $|\beta_{iso}|$ is less than at positive angles of attack β. The maximum time between isothermal regimes is observed at initial time instants and amounts to 5.4 and 0.7 s for $\omega_f = 5$ and 40 deg/s, respectively (Figs. 4 and 5). The process of the transition to the isothermal regime is prolonged as compared to subsequent ones due to the strong aerodynamic heating acting on the body at initial time instants; it also determines the difference in values of $|\beta_{iso}|$ for positive and negative angles of attack at subsequent time instants.

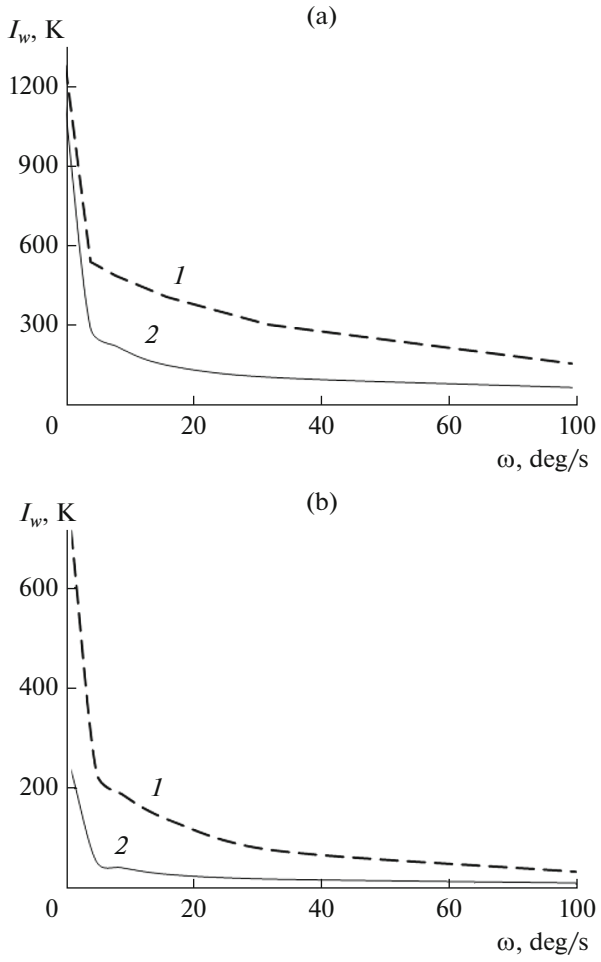

Fig. 8. Integrated surface temperature gradient as a function of the angular velocity of body oscillations at $V_\infty =$ (a) 5000 and (b) 3000 m/s.

To study the effect of body oscillations on heat transfer in the heat protection material in more detail, let us introduce the following quantity:

$$I_w = \frac{1}{t_z - t_0}\int_0^t [\Psi_{max}(t) - \Psi_{min}(t)]\,dt.$$

As seen from the formula presented above, the quantity I_w is numerically equal to the area of the region (hatched in Fig. 4) between the generators bounding the solution of the problem and characterizing the integrated difference of temperatures on the body surface normalized to the time interval of the flight. Figure 8 shows the integrated temperature difference on the body surface as a function of the velocity of oscillations during the considered time interval from $t = t_0$ to $t = t_z$ for $V_\infty = 3000$ and 5000 m/s, respectively. These dependences were constructed based on the results of a series of 24 calculations corresponding to variation of the incoming flow velocity

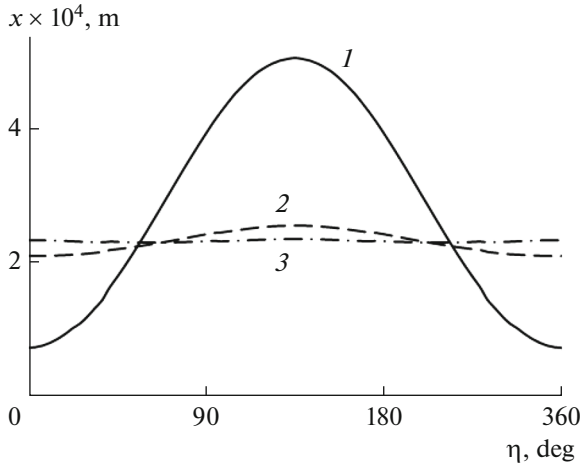

Fig. 9. Burnout depth of the material as a function of the circumferential coordinate for the carbon composite at $V_\infty = 5000$ m/s: $\omega_f = 0$ (*1*), (*2*) 5, and (*3*) 40 deg/s.

$V_\infty = 3000$ and 5000 m/s, angular velocity $\omega_f = 0$, 5, 10, 20, 40, and 100 deg/s, and materials (carbon composite and graphite). Curves *1* in Fig. 8 correspond to the carbon composite; curves *2* correspond to graphite. As seen from Fig. 8, even at small angular velocities of oscillations ($\omega_f = 5$ deg/s), the temperature difference heavily decreases (for the carbon composite, by 58–67%; for graphite, down to 74–76%) as compared to the case of the motion with a constant angle of attack. To reach the level of the temperature difference on the graphite surface, e.g., $I_w < 300$ K with carbon composite as the heat-protection material, a higher body oscillation velocity $\omega_f = 40$ deg/s is required, while $\omega_f = 5$ deg/s is sufficient for graphite (Fig. 8).

As a result, in the presence of oscillations, the change in the body shape as a consequence of linear ablation of the material from the surface due to aerodynamic heating will be more uniform (Fig. 9). Curves *1–3* in Fig. 9 correspond to carbon composite and $\omega_f = 0$, 5, and 40 deg/s. In the presence of oscillations $\omega_f = 5$–100, the average values of distribution functions of the burnout depth $x(\eta)$ presented in Fig. 9, as compared to $\omega_f = 0$ deg/s, are 18–19% lower. The maximum deviation of the function $x(\eta)$ from its average values of 76% for $\omega_f = 0$ decreases to 1.5% for $\omega_f = 40$ deg/s. This suggests that oscillations in general lead to a smaller change in the shape of the flying vehicle both in qualitative and quantitative aspects.

CONCLUSIONS

Within the framework of the conjugate formulation of the problem, the integrated effect of a regular oscillatory motion of a body on heat flux in the heat-protection coating was estimated. It was shown that the temperature difference on the body surface considerably decreases (by 58–78% depending on the material and conditions of the flow), even at small values of the angular velocity of oscillations. It was also shown that isothermal regimes of the body surface appear with irregular cyclicity. The velocity of the change of the attack angle $\omega_f \geq 5$ deg/s leads to a more uniform and lesser (by 18–19%) change in the shape of the flying vehicle as compared to the motion with a constant angle of attack. This ensures better preservation of the aerodynamic characteristics of the flying vehicle and less linear ablation of the heat-protection material.

FUNDING

This work was supported by the Mendeleev Foundation, project no. 8.2.15.2018.

REFERENCES

1. Hoffman, G.H. and Plastzer, M.F., *AIAA J.*, 1966, vol. 4, no. 2, p. 370.
2. Telionis, D. and Gupta, T., *AIAA J.*, 1977, vol. 15, no. 7, p. 974.
3. Zinchenko, V.I., Efimov, K.N., and Yakimov, A.S., *High Temp.*, 2007, vol. 45, no. 5, p. 681.
4. Efimov, K.N., Ovchinnikov, V.A., Yakimov, A.S., and Gaar, S.A., *High Temp.*, 2019, vol. 57, no. 1, p. 73.
5. Grishin, A.M. and Fomin, V.M., *Sopryazhennye i nestatsionarnye zadachi mekhaniki reagiruyushchikh sred* (Conjugate and Nonstationary Problems of Mechanics of Reacting Media), Novosibirsk: Nauka, 1984.
6. Efimov, K.N., Ovchinnikov, V.A., and Yakimov, A.S., *Thermophys. Aeromech.*, 2017, vol. 24, no. 5, p. 657.
7. Efimov, K.N., Ovchinnikov, V.A., and Yakimov, A.S., *AIAA J.*, 2018, vol. 56, no. 2, p. 743.
8. Efimov, K.N., Ovchinnikov, V.A., and Yakimov, A.S., *High Temp.*, 2018, vol. 56, no. 2, p. 239.
9. Grishin, A.M., Golovanov, A.N., Zinchenko, V.I., Efimov, K.N., and Yakimov, A.S., *Matematicheskoe i fizicheskoe modelirovanie teplovoi zashchity* (Mathematical and Physical Modeling of Thermal Protection), Tomsk: Tomsk. Gos. Univ., 2011.
10. Polezhaev, Yu.V. and Yurevich, F.P., *Teplovaya zashchita* (Thermal Protection). Moscow: Energiya, 1976.
11. Lunev, V.V., Magomedov, K.M., and Pavlov, V.G., *Giperzvukovoe obtekanie prituplennykh konusov s uchetom ravnovesnykh fiziko-khimicheskikh prevrashchenii* (Hypersonic Flow around Blunt Cones Taking into Account Equilibrium Physicochemical Transformations), Moscow: Vychislit. Tsentr Akad. Nauk SSSR, 1968.
12. Gorskii, V.V. and Zaprivoda, A.V., *High Temp.*, 2014, vol. 52, no. 2, p. 230.
13. Patankar, S.V. and Spalding, D.B., *Heat and Mass Transfer in Boundary Layers*, London: Morgan–Grampian, 1967.

14. Sebesi, T., *AIAA J.*, 1970, vol. 8, no. 12, p. 48.
15. Dhawan, D. and Narasimha, R., *J. Fluid Mech.*, 1958, no. 3, p. 418.
16. Grishin, A.M., Zinchenko, V.I., Efimov, K.N., Subbotin, A.N., and Yakimov, A.S., *Iteratsionno-interpolyatsionnyi metod i ego prilozheniya* (Iterative Interpolation Method and Its Applications), Tomsk: Tomsk. Gos. Univ., 2004.
17. Feldhuhn, R.N., *AIAA Pap.* 76-119, 1976.
18. Widhopf, G.F. and Hall, R., *AIAA J.*, 1972, vol. 10, p. 1318
19. Samarskii, A.A., *Vvedenie v teoriyu raznostnyh skhem* (Introduction to the Theory of Difference Schemes), Moscow: Nauka, 1971.
20. Gofman, A.G. and Grishin, A.M., *J. Appl. Mech. Tech. Phys.*, 1984, vol. 25, no. 4, p. 598.
21. Baker, R.L., *AIAA J.*, 1977, vol. 15, no. 10, p. 1391.
22. Andrievskii, R.A., *Poristye metallokeramicheskie materialy* (Porous Cermet Materials), Moscow: Metallurgiya, 1964.
23. Buchnev, L.M., Smyslov, A.I., Dmitriev, I.A., et al., *High Temp.*, 1987, vol. 25, no. 6, p. 816.
24. Alifanov, O.M., Tryanin, A.P., and Lozhkin, A.L., *J. Eng. Phys.*, 1987, vol. 52, no. 6, p. 340.
25. Sosedov, V.P., *Svoistva konstruktsionnykh materialov na osnove ugleroda. Spravochnik* (Properties of Carbon-Based Structural Materials: Handbook), Moscow: Metallurgiya, 1975.

Translated by A. Nikol'skii